Tunable passively *Q*-switched ytterbium-doped fiber laser with mechanically exfoliated GaSe saturable absorber

H. Ahmad*, S. N. Aidit, S. I. Ooi, and Z. C. Tiu

Photonics Research Centre, University of Malaya, Kuala Lumpur 50603, Malaysia
**Corresponding author: harith@um.edu.my*

Received October 17, 2017; accepted November 16, 2017; posted online February 5, 2018

A tunable passively *Q*-switched ytterbium-doped fiber laser using few-layer gallium selenide (GaSe) as a saturable absorber (SA) is demonstrated. The few-layer GaSe SA, which is fabricated by the mechanical exfoliation method, is able to generate a *Q*-switched fiber laser that has a maximum repetition rate of 92.6 kHz and a minimum pulsed width of 2.3 μs. The highest pulse energy exhibited by the generated pulse is 18.8 nJ with a signal to noise ratio of ~40 dB. The tunability of the proposed laser covers from 1042 to 1082 nm, giving a tuning range of 40 nm.

OCIS codes: 060.3510, 140.3540, 140.3615.
doi: 10.3788/COL201816.020014.

Q-switched fiber lasers have emerged as a powerful platform for a wide range of applications, including optical imaging, sensing, and the area of optical spectroscopy. While most conventional *Q*-switched fiber laser designs employ acousto-optic or electro-optic modulators[1] to achieve the desired pulsed output, these systems also have a number of inherent limitations, in particular, the need for complex electronics, which increases the overall bulk, complexity, and cost of the system. In this regard, passively *Q*-switched fiber lasers have recently garnered increasing interest as an attractive and cost-effective alternative towards generating compact and cost-effective pulsed fiber lasers.

Q-switching can be realized using a variety of saturable absorbers (SAs) in different gain media, such as thulium (Tm)[2,3], erbium (Er)[4,5], and ytterbium (Yb)[6,7] fibers. Typically, the choice of SA was semiconductor SA mirrors (SESAMs), which was a highly dependable technology with significant advantages, including controllable recovery time, saturation energy, and absorption loss. However, their fabrication complexity invariably caused SESAMs to become very costly and also only usable over a particular wavelength range, thus substantially limiting their applications[8,9]. To overcome this, researchers instead turned towards two-dimensional (2D) materials, which have shown significant promise for use as an SA. Graphene, in particular, proved to be a highly potential SA due to its ultra-wideband response, as a result of its gapless nature and very fast optical response[10–12]. However, the use of graphene as an SA is limited due to its zero band gap and weak absorption coefficient. In order to overcome this limitation, other materials have also been explored for their potential as SA materials, including transition metal dichalcogenides (TMDs), such as tungsten disulphide (WS_2), molybdenum disulphide (MoS_2), and molybdenum diselenide ($MoSe_2$)[4,13–16].

Gallium selenide (GaSe), in particular, has shown considerable potential for use as an SA. Composed of vertically stacked Se-Ga-Ga-Se atom sheets held together by a weak van der Waals force[17–19], GaSe can complement graphene and other 2D materials due to its outstanding optoelectronic features, including a relatively low dark current ascribed to a high resistivity GaSe layered structure. This makes GaSe highly promising for transistor and photodetector applications[20–23]. Categorized as a p-type semiconductor, GaSe exhibits an indirect bandgap of 2.11 eV, which is only 25 meV lower than the direct bandgap[24,25]. Nevertheless, the difference between the direct and indirect band gaps is small enough that electrons can be easily transferred between the two energy levels with only a small amount of thermal energy. Furthermore, GaSe shows potential for nanophotonics device applications due to the absence of dangling bonds and a thermal stability of up to 600°C[20]. Furthermore, as a member of the TMD family, GaSe possesses a wide optical transparency that covers a wavelength range of 0.65 to 18 μm, as well as possessing high birefringence characteristics and high threshold damage for each different laser line[17]. In addition to this, GaSe is also a well-known nonlinear optical material and has been widely used for second-harmonic generation (SHG) applications[26,27]. However, to date, it has not yet been fully explored as an SA for pulse generation in fiber lasers despite its unique nonlinear optical properties.

In this study, mechanically exfoliated GaSe is fabricated and used as an SA for *Q*-switched pulse generation. The optical characteristics of the GaSe-based SA are obtained, and the SA is integrated into an Yb-doped fiber laser (YDFL) for operation in the 1.0 μm region. Using mechanical exfoliation, thin layers of 2D GaSe are easily obtained from a bulk GaSe crystal, thereby making the SA fabrication process extremely simple and cost-effective.

To the best of authors' knowledge, this is the first time that a passively Q-switched fiber laser has been demonstrated with GaSe as an SA for operation in the 1.0 μm region. The proposed laser has significant potential for a wide range of applications, particularly for medical, chemical, and biological sensing.

The GaSe-based SA is prepared by mechanical exfoliation, a well-known and understood process used with graphene[28,29]. Fabricating the SA by mechanical exfoliation is simple and reliable, and does not involve costly instruments or additional chemicals. This method has also been widely implemented to other 2D materials, including black phosphorus (BP)[30] and topological insulators (TIs)[31], mainly for pulsed fiber laser applications. The mechanically exfoliated GaSe SA is characterized using Raman spectroscopy, and the obtained spectrum is compared to that of bulk GaSe in Fig. 1(a). Three prominent Raman modes typical to those of bulk GaSe at ~150, ~214, and ~324 cm^{-1} are observed. These peaks are consistent with previous reports[20], indicating that the bulk GaSe sample has a high level of purity. As the thickness of the sample is reduced, the peak intensity decreases significantly or vanishes completely. This is shown in a few-layer GaSe spectrum, where there is only a small peak that appears at 321 cm^{-1}, which is red-shifted compared to 324 cm^{-1} in bulk GaSe. Comparing the shifting of the Raman spectrum peaks with previous works[21,32], we estimate the thickness of the GaSe nanosheet to be 3–5 layers. Moreover, the nonlinear properties of the GaSe SA are characterized using the twin detector technique with a homemade fiber laser having a pulse duration of 0.70 ps and a repetition rate of 27.9 MHz at a central wavelength of 1560 nm as the pulse seed laser. It can be seen from the nonlinear absorption curve in Fig. 1(b) that the GaSe-based SA has a modulation depth of ~10% and a saturation intensity of ~0.024 $MW \cdot cm^{-2}$. The saturation intensity (I_{sat}) of the GaSe sample is much lower compared to the I_{sat} of other materials, such as MoS_2[15], WS_2[33], and a TI SA mirror[34]. The wide variation of I_{sat} could be attributed to the different fabrication techniques that result in different sizes of the material and quality of the SA[35]. Additionally, field emission scanning electron microscopy (FESEM) is performed using a Hitachi SU8200 ultra high-resolution scanning electron microscope. The characterization provides the topographical and structural details of the surface of the sample. Figure 1(c) shows that the surface consists of few-layer GaSe flakes after they are exfoliated. The chemical composition of the sample is determined through energy dispersive X-ray (EDX) microscopy and is shown in Fig. 1(d), confirming the presence of Ga and Se with a weight by percentage (wt.%) of 52.61% and 47.39%, respectively.

The setup for a passively Q-switched YDFL is shown in Fig. 2. The gain medium is configured as a ring cavity and is pumped by an Oclaro LC96A74P-20R laser diode (LD) with a central wavelength of 974 nm and a maximum output power of 600 mW. The output of the LD is injected into the cavity through the 980 nm port of a 980/1060 nm wavelength division multiplexer (WDM), with the common port of the WDM fusion spliced to a 70-cm-long DF1100 Yb-doped fiber (YDF). The YDF is manufactured by Fibercore and has a peak absorption of 1300 $dB \cdot m^{-1}$ at 977 nm. The other end of the YDF is spliced to the input port of a 1.0 μm isolator, which is used to ensure that the signal in the cavity travels in only one direction. The output port of the isolator is connected to the SA assembly. The SA assembly consists of the GaSe-based thin film SA sandwiched between two fiber ferrules, using an optical fiber adaptor, and has a total insertion loss of 7.46 dB. The SA assembly is then connected to a tunable bandpass filter (TBPF, Agiltron Inc.) and subsequently to the input port of a 90/10 optical coupler (OC). The TBPF has a typical tuning range of 40 nm with a resolution of 0.1 nm. The 90% port of the OC is connected to the 1060 nm port of the WDM, thereby completing the optical circuit. The 10% port is used to extract a sample of the signal for analysis, with optical

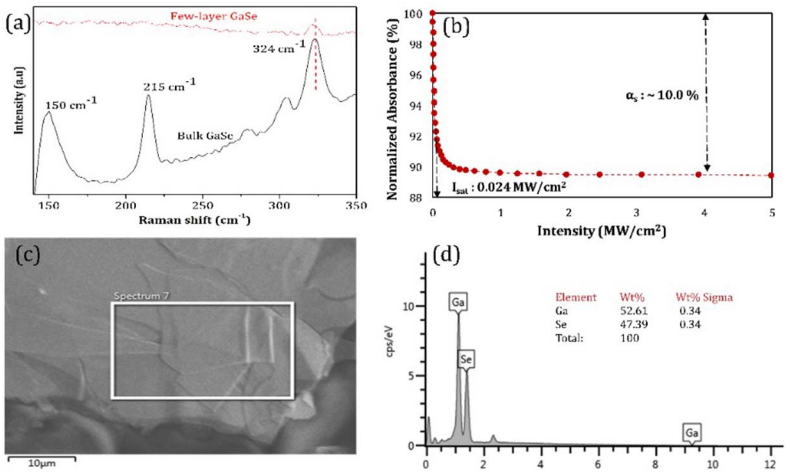

Fig. 1. Material characterization of mechanically exfoliated GaSe SA. (a) Raman spectrum, (b) nonlinear optical profile, (c) FESEM image, and (d) EDX analysis.

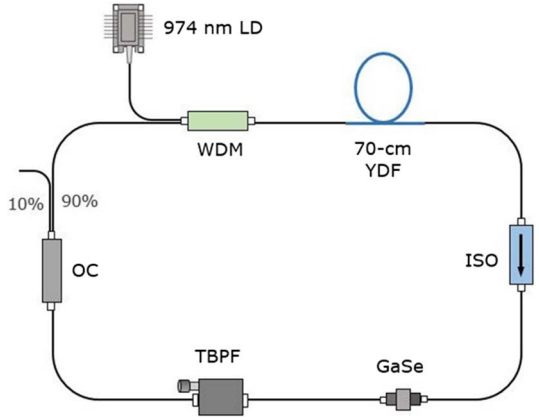

Fig. 2. Cavity configuration of a Q-switched YDFL.

characteristics being determined by a Yokogawa AQ6370B optical spectrum analyzer (OSA), and the pulse characteristics determined by a Yokogawa DLM2054 oscilloscope (OSC) and an Anritsu MS2683A radio-frequency spectrum analyser (RFSA).

The proposed YDFL initially operates in the continuous wave (CW) regime, with Q-switching operation being realized only with the incorporation of the GaSe-based SA into the ring cavity. By exploiting the nonlinear characteristics of the SA, the loss and Q-factor of the laser cavity are modulated to generate a stable Q-switched pulse train. Self-starting Q-switched pulses are realized at a threshold power of 158 mW, with Fig. 3 summarizing the typical output of the Q-switched YDFL at 1040 nm wavelength and 260 mW pump power. The pulses observed have a repetition rate of 92.6 kHz and a full width at half-maximum (FWHM) pulse duration of 2.3 μs, as shown in Figs. 3(a) and 3(b), respectively. Figure 3(c) gives the radio-frequency (RF) spectrum of the laser with a high signal to noise ratio (SNR) of ~40 dB, which indicates that the laser is operating in a relatively stable regime. The inset of Fig. 3(c) provides the full frequency spectrum of the pulses, covering the fundamental frequency at a full span of 500 kHz.

As the characteristics of the Q-switched pulses generated are dependent on the nonlinear dynamics of the gain medium and the SA, they are also by extension dependent on the input pump power. In this manner, a greater pump provides more gain to the gain medium, which, in turn, allows the laser to operate at higher repetition rates with shorter output pulses. Figure 4(a) shows the effect of the pump power on the repetition rate and pulse width of the generated output. From the figure, it can be seen that as the pump power is raised from 158 to 260 mW, the repetition rate, in turn, increases from 71.8 to 92.6 kHz, whereas the pulse width narrows from 3.1 to 2.3 μs. Additionally, the average output power and pulse energy increase linearly against the pump power, with the highest average output power of 1.7 mW and pulse energy of 18.8 nJ, limited only by the available pump power. These trends are given in Fig. 4(b). Higher average output

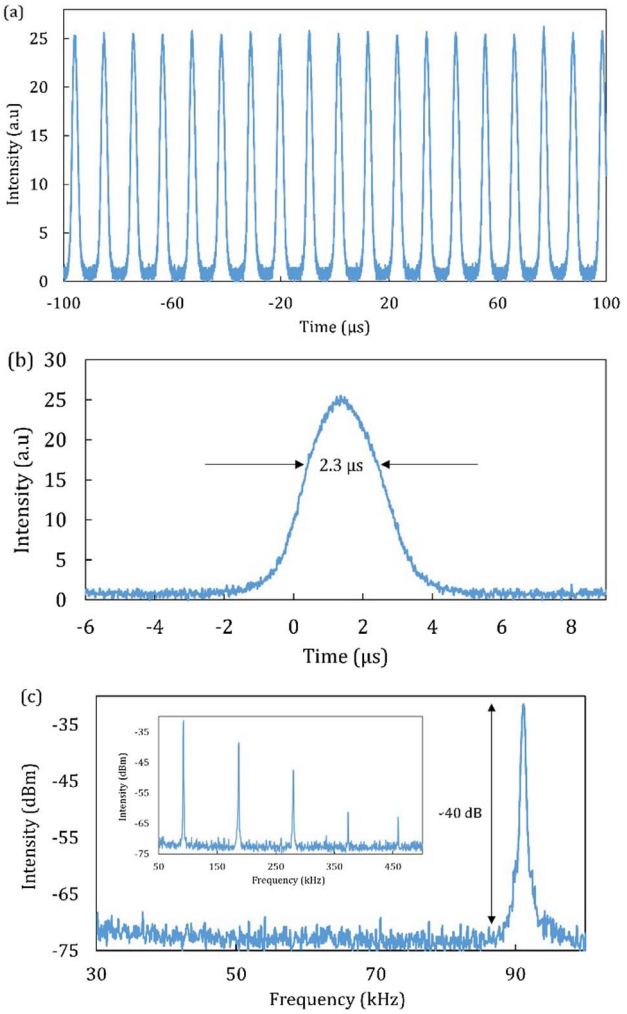

Fig. 3. Typical characteristics of a Q-switched YDFL at pump power of 261 mW. (a) Pulse train, (b) single pulse profile, and (c) RF spectrum of fundamental frequency at 92.6 kHz.

powers could be achieved by further optimizing the laser cavity, for instance, by enhancing the pump power. Further pump power scale-ups result in higher average output powers, as it has a linear relationship, as depicted in Fig. 4(b). Moreover, the average output power can also be improved by optimizing the YDF. In addition, the pulse energy, as illustrated in Fig. 4(b), does not show any indications of saturation. This indicated the possibility of further power scalability at higher pump powers becomes available. It can also be inferred from this that the fabricated SA exhibits a high damage threshold.

The incorporation of the TBPF into the cavity allows for the central wavelength of the pulsed laser to be easily tuned.

For this work, continuous Q-switching operation with a stable output pulse train is achieved from 1042 to 1082 nm, giving a tuning range of 40 nm. It must be noted that this tuning range is limited only by the TBPF and not the SA or other components of the fiber cavity. While short, the tuning range of this work is comparable to that reported by Woodward *et al.*[35] Figure 5 shows Q-switched

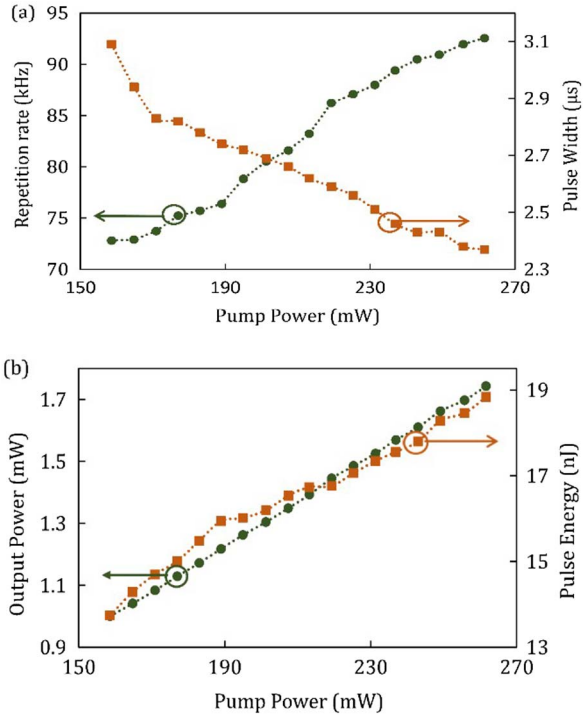

Fig. 4. Variation of *Q*-switched pulse parameters (a) repetition rate and pulse width, and (b) output power and pulse energy against pump power.

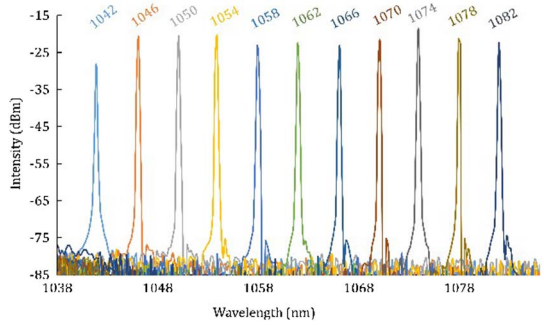

Fig. 5. *Q*-switched output spectra at different wavelengths, covering a tuning range of 40 nm (1042–1082 nm).

output spectra at different central wavelengths achieved by adjusting the TBPF. The variation observed in the spectral intensity is owing to the fact that amplifier gain varies with the wavelength.

Table 1 compares the performance of the proposed YDFL with a GaSe-based SA of this work against those of other similar systems, but by utilizing different SAs. From the table, it can be seen that the YDFL with the GaSe-based SA is able to generate an output with a repetition rate of 92.6 kHz. This value is the highest obtained, with the next closest being those of zinc oxide and BP at only 50.0 and 44.8 kHz, respectively. The repetition rate is even lower when other materials are used to induce the *Q*-switching, including TMD-based SAs, such as WS_2, MoS_2, and TI:Bi_2Se_3, which all have repetition rates of below 50.0 kHz. In addition to this, although the pulse energy obtained in this work is not as high as that obtained by Woodward *et al.*[35] using a MoS_2-based SA, its performance is still comparable to WS_2 and TI:Bi_2Se_3-based SA's and is higher than reported with those systems utilizing ZnO and BP-based SAs. Also crucial, this work is among the few that reports a *Q*-switched YDFL with tuning capabilities, with the only other being that using the MoS_2-based SA. With tuning range of 40 nm, the proposed system offers various advantages for tuned pulsed outputs, especially for sensing applications.

In this work, stable *Q*-switching operation is demonstrated in a YDFL incorporating a GaSe-based SA. The SA is fabricated by mechanically exfoliating GaSe thin films from a bulk GaSe crystal and then sandwiching the thin films between two fiber ferrules. The *Q*-switched laser has a tuning range of 40 nm with a maximum repetition rate of 92.6 kHz and a minimum pulse width of 2.3 μs. The highest pulse energy is recorded to be 18.8 nJ with an SNR of ~40 dB. Due to its reliable performance, easy fabrication, and low cost properties, GaSe shows significant promise for pulsed fiber laser, nonlinear photonics, and optoelectronics applications.

We thank the Ministry of Higher Education, MOHE, for funding this work under Grant LRGS (2015) NGOD/UM/KPT and the University of Malaya, UM, for funding this work under Grant RU 001 – 2017.

Table 1. Comparison of *Q*-switched YDFL Utilizing Different SAs.

SA	Max. Repetition Rate (kHz)	Min. Pulse Width (μs)	Max. Pulse Energy (nJ)	Tuning Range (nm)	Reference
ZnO	50	1.6	2.8	-	[36]
WS_2	36.7	3.2	13.6	-	[5]
MoS_2	74	2.8	122	40	[35]
Bi_2Se_3	29.1	1.9	17.9	-	[37]
BP	44.8	4	7.1	-	[38]
GaSe	92.6	2.3	18.8	40	This work

References

1. W. Li, H. Liu, J. Zhang, H. Long, S. Feng, and Q. Mao, Appl. Opt. **55**, 4584 (2016).
2. M. Chernysheva, C. Mou, R. Arif, M. AlAraimi, M. Rümmeli, S. Turitsyn, and A. Rozhin, Sci. Rep. **6**, 24220 (2016).
3. J. Liu, J. Xu, and P. Wang, Opt. Commun. **285**, 5319 (2012).
4. B. Chen, X. Zhang, K. Wu, H. Wang, J. Wang, and J. Chen, Opt. Express. **23**, 26723 (2015).
5. M. Zhang, G. Hu, G. Hu, R. C. T. Howe, L. Chen, Z. Zheng, and T. Hasan, Sci. Rep. **5**, 17482 (2015).
6. J. Liu, S. Wu, Q.-H. Yang, and P. Wang, Opt. Lett. **36**, 4008 (2011).
7. Z. Luo, Y. Huang, M. Zhong, Y. Li, J. Wu, B. Xu, and H. Xu, J. Lightwave Technol. **32**, 4679 (2014).
8. U. Keller, Nature **424**, 831 (2003).
9. U. Keller, K. J. Weingarten, F. X. Kärtner, D. Kopf, B. Braun, I. D. Jung, R. Fluck, C. Hönninger, N. Matuschek, and J. Aus Der Au, IEEE J. Sel. Top. Quantum Electron. **2**, 435 (1996).
10. A. Martinez and Z. Sun, Nat. Photon. **7**, 842 (2013).
11. M. Jiang, H. F. Ma, Z. Y. Ren, X. M. Chen, J. Y. Long, M. Qi, D. Y. Shen, Y. S. Wang, and J. T. Bai, Laser Phys. Lett. **10**, 55103 (2013).
12. W. J. Cao, H. Y. Wang, A. P. Luo, Z. C. Luo, and W. C. Xu, Laser Phys. Lett. **9**, 54 (2012).
13. R. I. Woodward, R. C. T. Howe, T. H. Runcorn, G. Hu, F. Torrisi, E. J. R. Kelleher, and T. Hasan, Opt. Express. **23**, 20051 (2015).
14. K. Wu, X. Y. Zhang, J. Wang, X. Li, and J. P. Chen, Opt. Express **23**, 11453 (2015).
15. Y. Huang, Z. Luo, Y. Li, M. Zhong, B. Xu, K. Che, H. Xu, Z. Cai, J. Peng, and J. Weng, Opt. Express. **22**, 25258 (2014).
16. S. Wang, H. Yu, H. Zhang, A. Wang, M. Zhao, Y. Chen, L. Mei, and J. Wang, Adv. Mater. **26**, 3538 (2014).
17. K. R. Allakhverdiev, M. Ö. Yetis, S. Özbek, T. K. Baykara, and E. Y. Salaev, Laser Phys. **19**, 1092 (2009).
18. Y. Wu, H. R. Fuh, D. Zhang, C. Coileáin, H. Xu, J. Cho, M. Choi, B. S. Chun, X. Jiang, M. Abid, M. Abid, H. Liu, J. J. Wang, I. V. Shvets, C. R. Chang, and H. C. Wu, Nano Energy **32**, 157 (2017).
19. V. Zólyomi, N. D. Drummond, and V. I. Fal'Ko, Phys. Rev. B **87**, 195403 (2013).
20. P. Hu, Z. Wen, L. Wang, P. Tan, and K. Xiao, ACS Nano **6**, 5988 (2012).
21. D. J. Late, B. Liu, H. S. S. R. Matte, C. N. R. Rao, and V. P. Dravid, Adv. Funct. Mater. **22**, 1894 (2012).
22. S. Lei, L. Ge, Z. Liu, S. Najmaei, G. Shi, G. You, J. Lou, R. Vajtai, and P. M. Ajayan, Nano Lett. **13**, 2777 (2013).
23. Y. Zhou, Y. Zhou, Y. Nie, Y. Liu, K. Yan, J. Hong, C. Jin, J. Yin, Z. Liu, and H. Peng, ACS Nano **8**, 1485 (2014).
24. V. Capozzi and M. Montagna, Phys. Rev. B **40**, 3182 (1989).
25. H. Huang, P. Wang, Y. Gao, X. Wang, T. Lin, J. Wang, L. Liao, J. Sun, X. Meng, Z. Huang, X. Chen, and J. Chu, Appl. Phys. Lett. **107**, 143112 (2015).
26. W. Jie, X. Chen, D. Li, L. Xie, Y. Y. Hui, S. P. Lau, X. Cui, and J. Hao, Angew. Chemie - Int. Ed. **54**, 1185 (2015).
27. V. G. Voevodin, O. V. Voevodina, S. A. Bereznaya, Z. V. Korotchenko, A. N. Morozov, S. Y. Sarkisov, N. C. Fernelius, and J. T. Goldstein, Opt. Mater. (Amst) **26**, 495 (2004).
28. A. Martinez, K. Fuse, and S. Yamashita, Appl. Phys. Lett. **99**, 121107 (2011).
29. Y. M. Chang, H. Kim, J. H. Lee, and Y. W. Song, Appl. Phys. Lett. **97**, 211102 (2010).
30. Y. Chen, G. Jiang, S. Chen, Z. Guo, X. Yu, C. Zhao, H. Zhang, Q. Bao, S. Wen, D. Tang, and D. Fan, Opt. Express **23**, 12823 (2015).
31. J. Sotor, G. Sobon, W. Macherzynski, P. Paletko, K. Grodecki, and K. M. Abramski, Opt. Mater. Express. **4**, 1 (2014).
32. X. Li, M.-W. Lin, A. A. Puretzky, J. C. Idrobo, C. Ma, M. Chi, M. Yoon, C. M. Rouleau, I. I. Kravchenko, D. B. Geohegan, and K. Xiao, Sci. Rep. **4**, 5497 (2015).
33. P. Yan, A. Liu, Y. Chen, H. Chen, S. Ruan, C. Guo, S. Chen, I. L. Li, H. Yang, J. Hu, and G. Cao, Opt. Mater. Express **5**, 479 (2015).
34. P. Yan, H. Chen, K. Li, C. Guo, S. Ruan, J. Wang, J. Ding, X. Zhang, and T. Guo, IEEE Photon. J. **8**, 1500506 (2016).
35. R. I. Woodward, E. J. R. Kelleher, R. C. T. Howe, G. Hu, F. Torrisi, T. Hasan, S. V. Popov, and J. R. Taylor, Opt. Express **22**, 31113 (2014).
36. H. Ahmad, M. A. M. Salim, M. F. Ismail, and S. W. Harun, Laser Phys. **26**, 115107 (2016).
37. Z. Luo, Y. Huang, J. Weng, H. Cheng, Z. Lin, B. Xu, Z. Cai, and H. Xu, Opt. Express **21**, 29516 (2013).
38. H. Ahmad, M. A. M. Salim, K. Thambiratnam, S. F. Norizan, and S. W. Harun, Laser Phys. Lett. **13**, 95103 (2016).